JACS
JOURNAL OF THE AMERICAN CHEMICAL SOCIETY
pubs.acs.org/JACS
Article

Achieving High Photo/Thermocatalytic Product Selectivity and Conversion via Thorium Clusters with Switchable Functional Ligands

Qian Niu, Qing Huang, Tao-Yuan Yu, Jiang Liu,* Jing-Wen Shi, Long-Zhang Dong, Shun-Li Li, and Ya-Qian Lan*

Cite This: https://doi.org/10.1021/jacs.2c08258
Read Online

ABSTRACT: Structural exploration and functional application of thorium clusters are still very rare on account of their difficult synthesis caused by the susceptible hydrolysis of thorium element. In this work, we elaborately designed and constructed four stable thorium clusters modified with different functionalized capping ligands, **Th_6-MA**, **Th_6-BEN**, **Th_6-C8A**, and **Th_6-Fcc**, which possessed nearly the same hexanuclear thorium-oxo core but different capabilities in light absorption and charge separation. Consequently, for the first time, these new thorium clusters were treated as model catalysts to systematically investigate the light-induced oxidative coupling reaction of benzylamine and thermo-driven oxidation of aniline, achieving >90% product selectivity and approximately 100% conversion, respectively. Concurrently, we found that thorium clusters modified by switchable functional ligands can effectively modulate the selectivity and conversion of catalytic reaction products. Moreover, catalytic characterization and density functional theory calculations consistently indicated that these thorium clusters can activate O_2/H_2O_2 to generate active intermediates $O_2^{\cdot-}/HOO^{\cdot}$ and then improved the conversion of amines efficiently. Significantly, this work represents the first report of stable thorium clusters applied to photo/thermotriggered catalytic reactions and puts forward a new design avenue for the construction of more efficient thorium cluster catalysts.

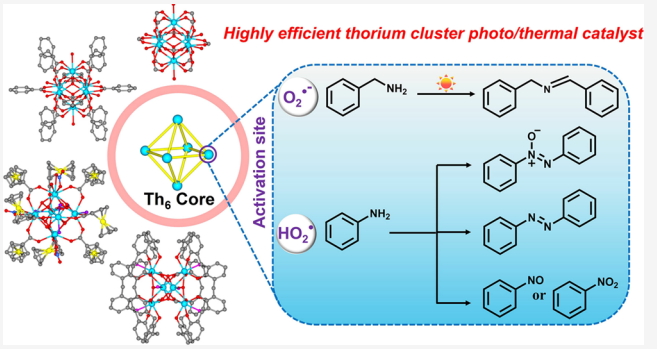

INTRODUCTION

As relatively abundant actinides on earth, thorium and its derivatives have manifested critical applications in nuclear energy, medical, and industrial fields because of their radiation resistance, high temperature resistance, and high thermal conductivity.[1−5] However, the relatively low structural variability of these materials restricts their development to some extent in more potential applications.[6−8] The development of thorium-based coordination compounds provides more possibilities to overcome these restrictions, because more structural variations and functional modulations can be readily implemented through the diverse coordination numbers and intriguing coordination modes of thorium as well as coordination of different functional ligands.[9] Particularly, thorium-based metal−organic frameworks (Th-MOFs) have been tuned for applications in gas adsorption, ion exchange, and radiation resistance through coordination modification with different organic ligands.[10−17] Nevertheless, the application of thorium-based functionalized materials (including thorium-based complexes) in the field of catalysis is still largely unexplored.[18−23] To date, a mere handful of Th-MOFs have been reported to be applied as heterogeneous catalysts for CO_2 cycloaddition and photocatalytic oxidation of 2-chloroethyl ethyl sulfide.[24−26]

From the perspective of catalysis, compared with Th-MOFs, thorium-based molecular compounds (such as thorium clusters) can be employed as homogeneous or heterogeneous catalysts. Therefore, they have greater potential to expose more catalytically active sites and catalytic specific surface area in principle, which is more favorable for enhancing the corresponding catalytic reaction performance. Unfortunately, thorium clusters have not yet been adapted to any catalytic reactions, mainly because of the tremendous challenge in the synthesis of thorium clusters.[27,28] Especially when compared with titanium, zirconium, and hafnium clusters with similar physicochemical properties,[29] thorium clusters with well-defined structures are extremely rare.[30−32] This is due to the

Received: August 4, 2022

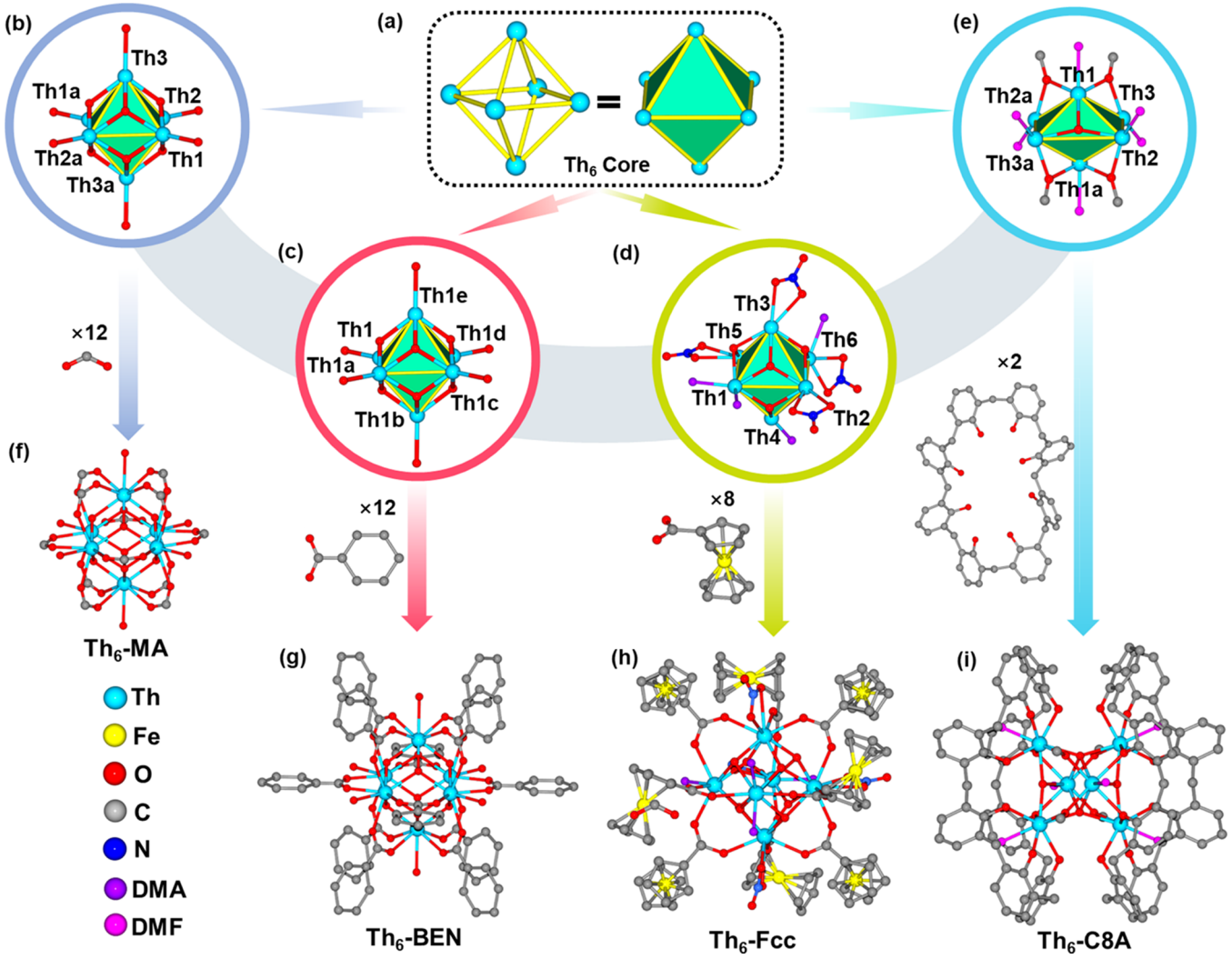

Figure 1. (a) Simplified model of Th_6 core. The hexanuclear thorium-oxo core of (b) **Th_6-MA**, (c) **Th_6-BEN**, (d) **Th_6-Fcc**, and (e) **Th_6-C8A**. The molecular structure view of (f) **Th_6-MA**, (g) **Th_6-BEN**, (h) **Th_6-Fcc**, and (i) **Th_6-C8A**. All hydrogen atoms are omitted for clarity, and purple represents *N*,*N*-dimethylacetamide molecules and pink represents *N*,*N*-dimethylformamide molecules.

strong Lewis acidity of Th^{4+} which makes its hydrolysis very rapid, leading to the coexistence of multimers (e.g., dimers, tetramers, hexamers, octamers, or decamers). This entails that it is difficult to form a uniform multicore cluster structure.[33] To cope with this challenge, one of the most effective strategies is to incorporate capping ligands to control the assembly process of thorium clusters.[34] Moreover, the coordination of functionalized capping ligands can further have a significant impact on the structural expansion and performance development of thorium clusters.

Herein, we designed and synthesized four different hexanuclear thorium clusters, $[Th_6O_4(OH)_4(HCOO)_{12}(H_2O)_6]$ (**Th_6-MA**, MA = Formic acid), $[Th_6O_4(OH)_4(BEN)_{12}(H_2O)_6]$ (**Th_6-BEN**, BEN = Benzoic acid), $[Th_6O_4(OH)_4(Fcc)_8(NO_3)_4(DMA)_4]$ (**Th_6-Fcc**, Fcc = Ferrocenecarboxylic acid), and $[Th_6(\mu_4\text{-}O)_2(\mu_3\text{-}O)_2(\mu\text{-}OCH_3)_4(C8A)_2(DMF)_6]$ (**Th_6-C8A**, C8A = Calix[8]arene) by incorporating different functionalized capping ligands during the synthesis. Among them, **Th_6-MA** has been reported in previous work.[35] With the coordination change of the functionalized organic ligands, the four hexanuclear thorium clusters exhibit different structural features, and they also show significant differences in their light absorption capacity (expanding from the UV to the visible region) as well as in their charge separation capacity. This makes it possible to consider these thorium clusters as a model system to systematically elucidate the changes in specific properties caused by the structure. Based on these advantages, we applied these thorium clusters as catalysts for photo or thermodriven amine oxidation reactions (including benzylamine oxidation and aniline oxidation) for the first time. In the photocatalytic benzylamine oxidative coupling reaction, **Th_6-C8A** exhibited the highest photocatalytic activity for benzylamine oxidation with a conversion efficiency as high as 99%, which was higher than that of **Th_6-Fcc** (87%) and much higher than that of **Th_6-MA** (6%) and **Th_6-BEN** (15%). Experimental characterization and theoretical calculation results evidenced that **Th_6-C8A** had a stronger charge separation ability and a stronger adsorption capacity for O_2 than the other three thorium clusters, which was beneficial to the activation of the reaction substrate and improve the photocatalytic conversion efficiency. When this model system was for aniline oxidation, highly selective conversion of different products can be reached by using different ligands functionalized with thorium clusters. **Th_6-MA** and **Th_6-BEN** can achieve a high selectivity of AB (94%, azobenzene) and AOB (100%, azoxybenzene) with approx-

https://doi.org/10.1021/jacs.2c08258
J. Am. Chem. Soc. XXXX, XXX, XXX−XXX

imately 100% conversion; **Th_6-Fcc** can afford a high selectivity of NSB (100%, nitrosobenzene) and NB (100%, nitrobenzene). Notably, **Th_6-C8A** as a catalyst can activate H_2O_2 to highly selectively oxidize aniline to form AOB (98%), NSB (93%), and AB (77%) with high conversion, respectively. The theoretical calculations indicated that the activation site of H_2O_2 was mainly on Th^{4+} sites, and the solvation effect can lead to different oxidation products of aniline by facilitating the production of Ph-NHOH intermediates. To the best of our knowledge, this is the first time that thorium cluster catalysts have been employed to realize the selective regulation of four different products in the aniline oxidation reaction. This work provides a new research strategy for the structural design and catalytic application (photocatalysis or thermocatalysis) of more effective thorium cluster catalysts.

RESULTS AND DISCUSSION

Synthesis and Structure of Thorium Clusters. Hexanuclear thorium clusters functionalized with different ligands, **Th_6-MA**, **Th_6-BEN**, **Th_6-C8A**, and **Th_6-Fcc**, were successfully synthesized via the hydrothermal method (see the Experimental Section) with relatively high yields (Figure S1), all of which are composed of similar Th_6 cores (Figure 1a). Single-crystal X-ray diffraction analysis (SCXRD) reveals that **Th_6-MA** crystallizes in the orthorhombic space group *Pccn* (Table S1), and its asymmetric unit involves three Th atoms (Th1, Th2, Th3), three μ_3-O/OH, six MA, and three water molecules (Figure S2). **Th_6-BEN** directs to a highly symmetric cubic *Im* $\bar{3}$*m* space group. There are one Th atom, 1/3 μ_3-O/OH, and one water molecule in the asymmetric unit of **Th_6-BEN** (Figure S3). Both colorless polyhedron-shaped **Th_6-MA** and **Th_6-BEN** consist of one $Th_6O_4(OH)_4^{12+}$ hexamer cluster decorated by 12 ligands (formic acid or benzoic acid) (Figure 1f,g). The $Th_6O_4(OH)_4^{12+}$ core is composed of six 9-coordinated Th atoms bridged by four μ_3-OH and four μ_3-O groups. Each Th atom shows a capped square antiprismatic geometry assembled with four μ_3-OH/μ_3-O atoms, four O atoms from formic acid or benzoic acid ligands, and one terminal O atom from a coordination water molecule (Figure 1b,c).

When MA and BEN ligands were replaced by Fcc ligands, orange red hexagon-shaped crystals of **Th_6-Fcc** with high crystallinity were formed in high yield. SCXRD analysis indicates that it crystallizes in a triclinic crystal system with the space group $P-\bar{1}$. As shown in Figures S4 and 1h, its asymmetric unit consists of a $Th_6O_4(OH)_4^{12+}$ hexamer cluster decorated by eight Fcc ligands, four *N*,*N*-Dimethylacetamide molecules, and four nitrates. One may note that although **Th_6-Fcc** shows a similar Th_6 core to **Th_6-MA** and **Th_6-BEN**, there are clearly different coordination numbers of Th atoms (Figure 1d). Except for the eight-coordinated Th1 and Th4 atoms, all the other Th atoms are nine-coordinated. When the thorium cluster was further modified with the C8A ligand, highly crystalline yellow strip-shaped crystals, **Th_6-C8A**, were fabricated in high yield. SCXRD analysis demonstrates that **Th_6-C8A** crystallizes in a monoclinic crystal system with the $P2_1/n$ space group. As illustrated in Figure S5, its asymmetric unit involves three Th atoms (Th1, Th2, Th3), one μ_3-O, 1/2 μ_4-O, one C8A ligand, three *N*,*N*-dimethylformamide molecules, and two OCH_3 groups. All Th atoms in the compound are eight-coordinated and consist of eight O atoms from μ_3-O, μ_4-O, μ-OCH_3, *N*,*N*-dimethylformamide, and C8A ligand. Two Th1 atoms are located on a plane of symmetric elements of mirror planes, which are connected via two μ_4-O atoms (Figure S6). Th1 atoms connect to Th2 and Th3 atoms through two μ_3-O atoms and two μ_4-O and four μ-OCH_3 groups to form hexanuclear thorium-oxo core ($[Th_6(\mu_4\text{-}O)_2(\mu_3\text{-}O)_2(\mu\text{-}OCH_3)_4]^{12+}$) (Figure 1e), which is different from the above-described $Th_6O_4(OH)_4^{12+}$. Then the overall metal-oxo core is firmly anchored in the cavity of two C8A ligands in which eight hydroxyl groups are coordinated to Th1, Th2, and Th3 atoms (Figure 1i). Notably, the metallic skeleton of **Th_6-C8A** is a $[Th^{IV}_6]$ (squashed) octahedron. Given that these clusters have a very similar thorium-oxo core and are modified by different functionalized organic ligands, they may serve as a model system to systematically study the effect of structure-induced functional changes on specific properties.

The experimental powder X-ray diffraction (PXRD) patterns of as-synthesized thorium clusters were in good agreement with the simulation results of crystallographic data, indicating that they had fine crystallinity and high purity (Figures S7–S11). The thermogravimetric analysis curves suggested that **Th_6-MA**, **Th_6-BEN**, **Th_6-C8A**, and **Th_6-Fcc** can maintain structure frameworks before 250, 200, 210, and 230 °C (Figure S12), respectively. Because of their excellent thermal stability, these thorium clusters are promising for thermal catalysis. Additionally, X-ray photoemission spectroscopy (XPS) was conducted to confirm the valence state of thorium atoms. The results implied that only Th(IV) existed in these clusters with binding energies of 344.1 eV ($4f_{5/2}$) and 334.7 eV ($4f_{7/2}$) (Figures S13 and S14).

Photocatalytic Performance toward Oxidative Coupling of Benzylamines. The light absorption capacity of these thorium clusters was evaluated first by solid-state ultraviolet–visible (UV–vis) absorption spectroscopy. As presented in Figure 2a, compared with **Th_6-MA** and **Th_6-BEN**, it was obvious that **Th_6-C8A** displayed a significant absorption extending to the visible region. Furthermore, **Th_6-Fcc** exhibited a wider light absorption range (400–600 nm). Based on UV–vis spectra, the bandgap energy values of the **Th_6-MA**, **Th_6-BEN**, **Th_6-C8A**, and **Th_6-Fcc** were reckoned to be 3.32, 4.12, 2.01, and 2.05 eV, which implied that these thorium clusters can display semiconductor-like properties (Figures S15). Subsequently, the highest occupied molecular orbital (HOMO) positions of thorium clusters were ascertained by ultraviolet photoelectron spectroscopy (UPS), from which the final HOMO positions of **Th_6-MA**, **Th_6-BEN**, **Th_6-C8A**, and **Th_6-Fcc** were estimated to be 7.54 (2.69 V vs NHE), 8.55 (3.70 V vs NHE), 6.25 eV (1.40 V vs NHE), and 6.25 eV (1.40 V vs NHE). The corresponding lowest unoccupied molecular orbital (LUMO) positions were calculated as 4.22 (**Th_6-MA**), 4.43 (**Th_6-BEN**), 4.24 (**Th_6-C8A**), and 4.20 (**Th_6-Fcc**) eV (Figure S16). To validate the accuracy of these results, Mott–Schottky electrochemical measurements were undertaken to confirm LUMO positions of the prepared clusters (Figures S17 and 2b). These results were consistent with the results of UPS. Obviously, these clusters have more positive HOMO levels, which permits them to be applied to some oxidation reactions such as amine oxidation reactions.

Based on the above advantages, we first utilized this model system for the photocatalytic benzylamine oxidative coupling reaction. Under visible light, **Th_6-MA** and **Th_6-BEN** exhibited poor catalytic activity in the coupling reaction, and although the photocatalytic activity of **Th_6-Fcc** was improved, its activity

https://doi.org/10.1021/jacs.2c08258
J. Am. Chem. Soc. XXXX, XXX, XXX–XXX

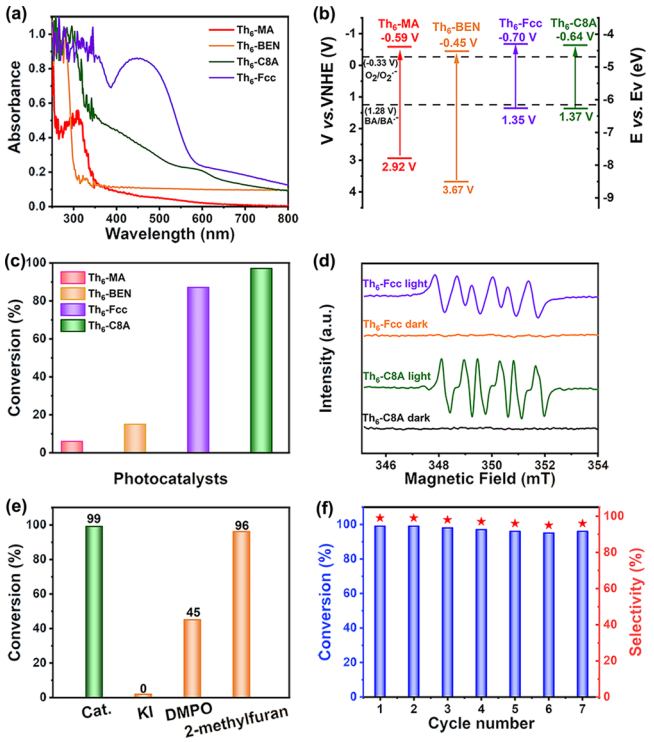

Figure 2. (a) UV−visible diffuse reflection spectra for four thorium clusters. (b) Energy band diagrams of four thorium clusters. (c) Conversion of oxidative coupling of benzylamine over four thorium clusters. (d) ESR spectra of **Th_6-C8A** and **Th_6-Fcc** in the presence of DMPO (a sextuplet is characteristic of DMPO-$O_2^{\cdot-}$ adducts). (e) Some comparative tests added to the corresponding sacrificial reagents. (f) Conversion and selectivity of oxidative of aniline with **Th_6-C8A** in seven repeating cycles.

was still lower than that of **Th_6-C8A** (Figures 2c and S18). Compared with the C8A ligand, **Th_6-C8A** displayed excellent catalytic performance with a conversion efficiency as high as 99% (2 times higher than that of the C8A ligand), along with the selectivity of N-benzylidenebenzylamine (BDA) approximately 99% (Table S2, entries 7−8). This may be associated with the charge separation ability of photocatalysts. In addition, photoluminescence (Figures S20 and S21) and time-resolved fluorescence decay techniques were performed to further investigate the charge separation efficiency and carrier lifetime of these clusters. As shown in Table S5, the fluorescence lifetime of **Th_6-C8A** (τ_{av} = 7.78 ns) was the longest among these thorium clusters and C8A ligands, implying that the separation efficiency of electron−hole pairs of **Th_6-C8A** was higher. Furthermore, electrochemical impedance spectroscopy (EIS) was carried out to verify the electron shuttle efficiency. The results of EIS showed that the impedance of **Th_6-C8A** was smaller than that of C8A. This revealed that the surface charge transfer rate of **Th_6-C8A** was faster and further proved that **Th_6-C8A** had higher charge separation efficiency (Figure S22). These results suggested that the functionalization of thorium clusters with different ligands could indeed improve the charge separation ability and further facilitated the photocatalytic oxidation reaction.

Thus **Th_6-C8A** becomes a better catalyst for the photocatalytic benzylamine coupling reaction in this model system. A series of control experiments were carried out to identify that O_2, light, and the photocatalyst were indispensable for this reaction (Table S2). Furthermore, the role of O_2 was confirmed by electron paramagnetic resonance (EPR) experiments in the photocatalytic oxidative coupling of benzylamine. Because of the formation of $O_2^{\cdot-}$ rather than $^1O_2$ in EPR experiments (Figure S23), **Th_6-C8A** likely proceeded via an $O_2^{\cdot-}$-mediated electron transfer pathway, rather than the $^1O_2$-assisted energy transfer route. In addition, visible-light-irradiated **Th_6-C8A** exhibited a sextuplet, while no EPR signals were detected in the dark, corroborating that $O_2^{\cdot-}$ was generated under light conditions (Figure 2d).[36] At the same time, some comparative experiments also demonstrated the important role of $O_2^{\cdot-}$ and holes by adding some sacrificial agents (Figure 2e).

Furthermore, the density functional theory (DFT) calculations were carried out to further explore the distinction in the photocatalytic performance of these four thorium clusters. In addition to the aforementioned charge separation efficiency, the adsorption capacity to reactant molecules is also an important factor affecting the reaction activity.[37−40] The calculation results showed that the adsorption energy of O_2 over these thorium clusters decreased in an order of **Th_6-MA** (0.09 eV) > **Th_6-BEN** (−0.18 eV) > **Th_6-Fcc** (−0.34 eV) > **Th_6-C8A** (−0.67 eV) (Figure 3b). This indicated that the

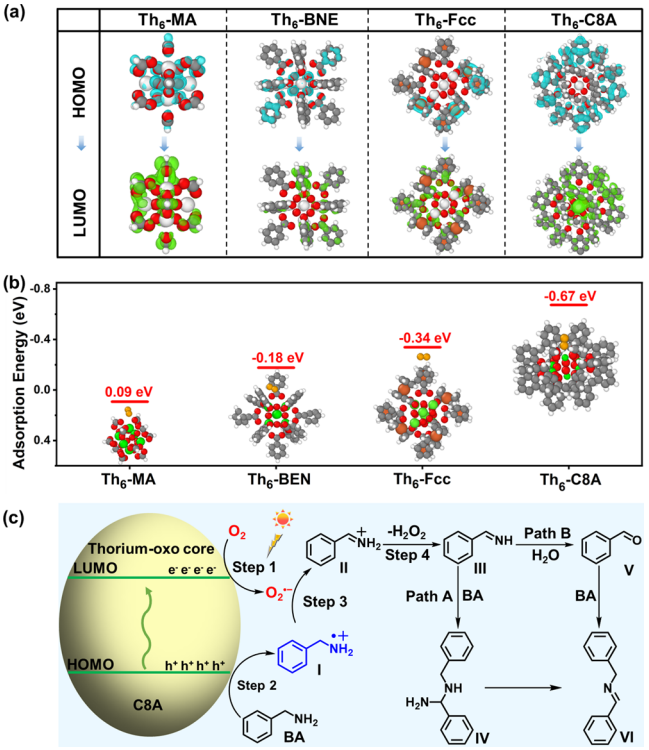

Figure 3. (a) DFT simulates the HOMO and LUMO of these four thorium clusters. (b) Oxygen adsorption energy barriers for **Th_6-MA**, **Th_6-BEN**, **Th_6-C8A**, and **Th_6-Fcc**. (c) Proposed reaction mechanisms for photocatalytic benzylamine oxidative coupling reaction.

order of photocatalytic reaction activity was **Th_6-C8A** > **Th_6-Fcc** > **Th_6-BEN** > **Th_6-MA**, which was consistent with experiments. We also found that compared to the other three thorium clusters, the LUMO and HOMO of **Th_6-C8A** were mainly located in the thorium-oxo core and ligands, respectively, which indicated the possible ligand-to-metal charge transfer process (Figure 3a). This meant that the thorium-oxo core also became the active site, because once C8A was stimulated by light, the thorium-oxo core will serve as

https://doi.org/10.1021/jacs.2c08258
J. Am. Chem. Soc. XXXX, XXX, XXX−XXX

an electron acceptor. On the basis of all the foregoing discoveries, the mechanism of oxidative coupling of benzylamine under visible light irradiation was proposed.[41−44] As shown in Figure 3c, the C8A ligand in **Th_6-C8A** can be excited by visible light, and the photogenerated electrons are transferred to the thorium-oxo core. The adsorbed benzylamine molecules were oxidized by photogenerated holes to form benzylamine radical cation(I), and simultaneously O_2 reacted with photogenerated electrons to generate $O_2^{\cdot-}$. Subsequently, intermediate I reacted with $O_2^{\cdot-}$ to produce intermediate II, which further converted into intermediate III. Then III can be readily attacked by another free benzylamine molecule to result in the formation of aminal(IV). After the release of ammonia, the final product *N*-benzylidenebenzylamine(VI) was produced (path A). In path B, III was hydrolyzed to obtain benzaldehyde(V), which was followed by condensation with another benzylamine to yield the coupling product.

The photocatalyst was removed from the reacted solution, and the residues of Th^{4+} ions in the filtrate were calculated to be only 0.025% (**Th_6-C8A**) by inductively coupled plasma (ICP) analysis. Additionally, no noticeable alteration appeared in the IR, PXRD, and XPS spectra of **Th_6-C8A** after reaction (Figures S26, S27, and S14), further proving that **Th_6-C8A** was the heterogeneous catalyst. Subsequently, the recycling tests confirmed that the **Th_6-C8A** could retain the catalytic activity and selectivity after seven cycles (Figure 2f). Meanwhile, the activity of **Th_6-C8A** on other benzylamine derivatives was performed under the same reaction conditions. The high conversion of benzylamine derivatives indicated that **Th_6-C8A** as a heterogeneous molecular catalyst had universality in the photocatalytic oxidative coupling of amines (Figure 6a).

Aniline Oxidation. Because of the presence of competitive oxidation and condensation reactions in the catalytic oxidation of amines, it is difficult to control the selectivity of the oxidation products (AB, AOB, NSB, NB).[45−47] As a result, the oxidation of cheap and abundant aniline into high-value products is a challenge in the industry.[48] To further explore the role of thorium clusters in the oxidation reaction, this model system was applied to the oxidation of aniline. It is expected that the functionalized thorium cluster model system can selectively modulate the aniline oxidation products toward AOB, AB, NSB, and NB. First, a series of solvents were screened, and the results obtained are shown in Tables S7−S10. We found that the highly controllable selectivity of the product can be accomplished by modifying different ligands on thorium clusters or adjusting the reaction solvent (Figure 4d). (1) When **Th_6-MA** was employed as a catalyst, AOB was the main product with low conversion efficiency in polar and protic solvents. The selectivity of NSB was improved in low polar and aprotic solvents, but the conversion efficiency needed to be further improved. In acetic acid, AB was obtained in significant quantities. (2) While using **Th_6-BEN** as the catalyst, AOB was the main product and achieved high conversion efficiency in low polar and aprotic solvents such as *n*-hexane, petroleum ether, and carbon tetrachloride. (3) When applying **Th_6-Fcc** as the catalyst, the products were diverse in polar and protic solvents. The main product was NSB in low polar and aprotic solvents (*N*-hexane-H_2O_2); NB became the main product in acetic acid. (4) When **Th_6-C8A** was taken as the catalyst, it was found that AOB was the main product in polar and protic solvents with high conversion efficiency, and a small amount of AB was formed (methanol-H_2O_2 system),

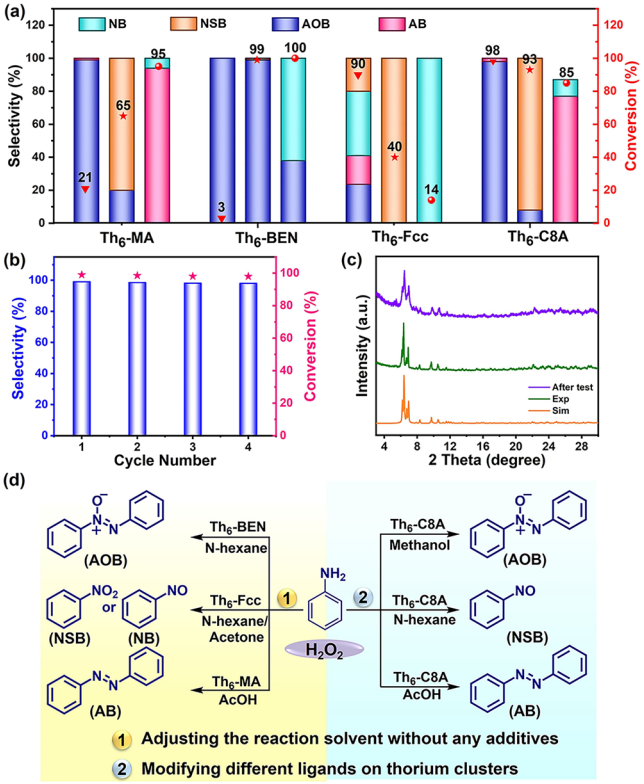

Figure 4. (a) Selective oxidation of anilines to azoxybenzenes, azobenzenes, and nitrosobenzenes with peroxide as the oxidant over four thorium clusters in an order of the methanol-H_2O_2 system/*N*-hexane-H_2O_2 system/AcOH-H_2O_2 system. (b) Conversion and selectivity of oxidative of aniline with **Th_6-C8A** in four repeating cycles. (c) PXRD patterns of **Th_6-C8A** before and after oxidative coupling of aniline in the methanol-H_2O_2 system. (d) Regulating product selectivity through two pathways over four thorium clusters.

while a large amount of AB could be detected (AcOH-H_2O_2 system) in acetic acid solvent. In more detail, the conditions in the methanol-H_2O_2 system were optimized (Table S11). As a result, high conversion efficiency of aniline and high selectivity of AOB can be achieved at room temperature. It was noted that aniline could be completely converted into AOB in a shorter time with the increase of temperature. By contrast, the utilization of low polar and aprotic solvents increased the selectivity of NSB (*N*-hexane-H_2O_2) (Figure 4a and Table S16).

Subsequent cycle tests showed that the catalytic activity of **Th_6-C8A** decreased very little after four cycles (Figure 4b). Moreover, the catalyst was removed from the solution after the reaction, and ICP results showed that the residual Th^{4+} in the filtrate was only 0.025% (**Th_6-C8A**). The PXRD, IR, and XPS spectra of the reused **Th_6-C8A** catalyst did not change significantly (Figures 4c, S32 and S33), which further proved that **Th_6-C8A** was the heterogeneous catalyst and maintained the structural integrity during the catalysis process. Then **Th_6-C8A** was selected as the catalyst for extending substrate experiments because of its high structural stability. In the methanol-H_2O_2 system, various amine derivatives including F, Cl, p-Me, m-Me, and o-Me were investigated. These derivatives can be oxidized to the corresponding azoxybenzenes in excellent yields (Figure 6b).

Next, the mechanism of aniline oxidation was disclosed by experiments. According to the available literature,[49,50] it is

https://doi.org/10.1021/jacs.2c08258
J. Am. Chem. Soc. XXXX, XXX, XXX−XXX

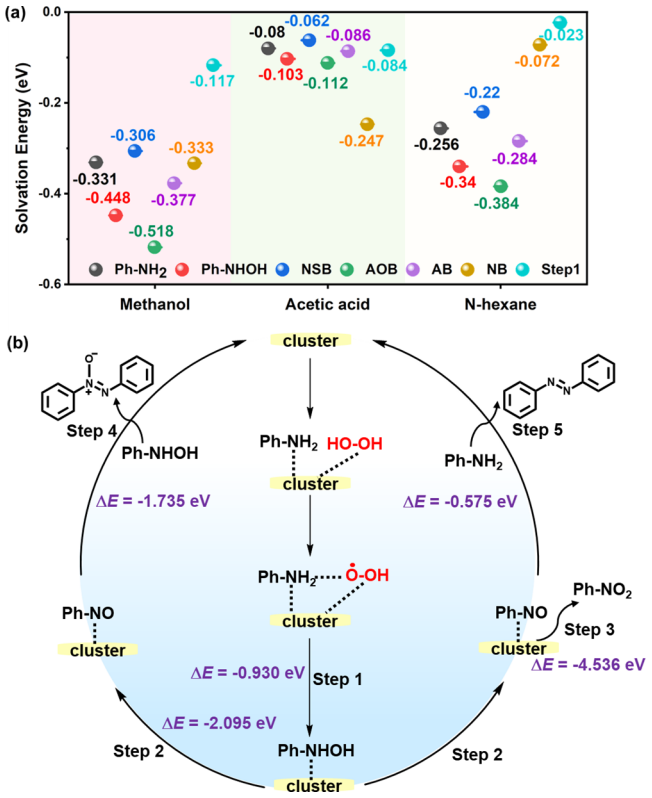

Figure 5. (a) Solvation energy of different substances and step 1 in methanol, acetic acid, and *n*-hexane. (b) Proposed reaction mechanisms for the aniline oxidation reaction through the nitrosobenzene intermediate. ΔE stands for reaction energy.

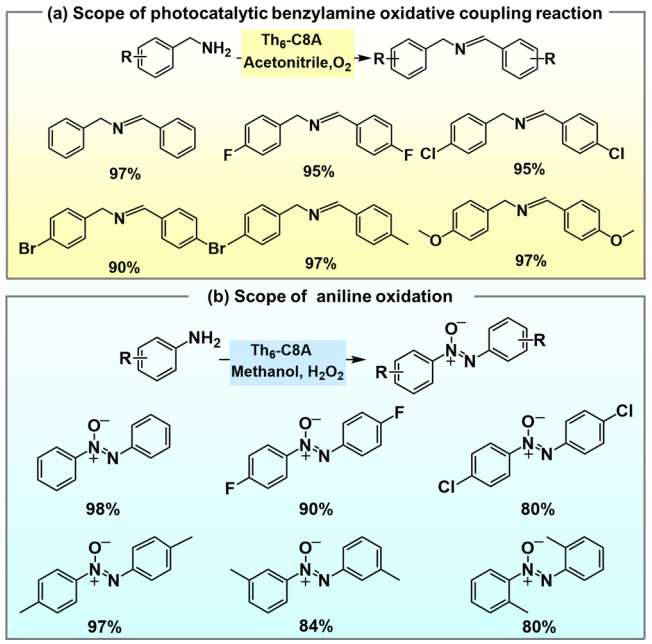

Figure 6. Reaction scope on (a) photocatalytic benzylamine oxidative coupling reaction: reaction conditions unless noted otherwise: substrate 0.1 mmol, catalysts 10 mg, solvent 2 mL of acetonitrile, reaction time 16 h under an O_2 atmosphere, in visible light (T = 25 °C), isolated yields. (b) Aniline oxidation: reaction conditions: aniline (0.1 mmol), **Th_6-C8A** (10 mg), methanol (1 mL), H_2O_2 (2 mmol, 30%w/w.), rt, 48 h, and isolated yields.

generally believed that the oxidation of aniline proceeds through two known mechanisms: the nitrosobenzene intermediate mechanism (Figure 5b) and the aniline radical mechanism. To identify the reaction mechanism, a series of comparative experiments were conducted. In the methanol-H_2O_2 system, the reaction proceeded normally when using 2,6-di-tert-butyl-4-methylphenol (BHT) as a radical scavenger (Table S14, entry 1), which indicated that the reaction does not proceed via the aniline radical. In addition, a large amount of NSB was detected in *n*-hexane solvent, further demonstrating the mechanism of aniline oxidation. These results suggested that the AOB and AB were generated undergoing the mechanism of nitrosobenzene (Table S14, Schemes S1 and S2).

DFT calculations were performed to confirm the actual active sites. As shown in Figure 5a, for these thorium clusters, the adsorption energy of H_2O_2 was lower on Th^{4+} sites than on bridging oxygen, suggesting that the adsorption sites of H_2O_2 were primarily on Th^{4+} sites, but not on bridging oxygen, except for **Th_6-BEN** (Figure S35). According to the above results, we proposed the mechanism of aniline oxidation on thorium clusters. These thorium clusters can adsorb and activate H_2O_2 to produce $HOO^{\cdot}$, which should be the active species for the reaction. Then $HOO^{\cdot}$ attacked aniline to generate phenylhydroxylamine (Ph-NHOH) (Figure 5b, step 1), which was readily oxidized to NSB (Figure 5b, step 2).[51] Then AOB was formed when the condensation reaction occurs between NSB and Ph-NHOH (Figure 5b, step 4), while NSB can also react with free aniline to afford AB (Figure 5b, step 5). In addition, NSB may be further oxidized to give NB (Figure 5b, step 3).

Subsequently, we also picked **Th_6-C8A** as the catalyst to research the effect of different solvents on the product selectivity by DFT calculations, and the associated reaction energies were marked in Figure 5b. The results displayed that the reaction energy of step 1 (−0.930 eV) is higher than that of step 2 (−2.095 eV), which implied that generated Ph-NHOH from Ph-NH_2 (step 1) could be the slowest step other than dimerization (step 4 and step 5). Therefore, the speed of this step can be determinative of the selectivity between AB and AOB. If this step is faster, AOB will be generated in priority; otherwise AB will be produced in consideration. The kinetic of step 1 can be tuned by solvents, and we can use the dielectric continuum model of COSMO (Computational Molecular Science) to calculate the associated solvation energies. As a result, the order of the solvation energy of step 1 is −0.023 eV (*n*-hexane) > −0.084 eV (acetic acid) > −0.117 eV (methanol), which implied that the solubilization effect can facilitate the step 1 (Figure 5a). In addition, we can read some additional messages from the solvation energy: the higher the permittivity, the faster step 1. It was inferred that AOB will be preferred in methanol solvent and AB will be more favored in acetic acid because the permittivity of methanol is higher than that of acetic acid (Table S6), which was consistent with the experimental observation. However, it seemed that *n*-hexane violated this trend. Its permittivity was the lowest, but it nearly will not produce AB. We speculated this was exceptional because the viscosity of *n*-hexane was so large that it inhibited the dimerization reaction (step 5). Therefore, the solvation dependent trend can be interpreted as the coeffect of the permittivity and the viscosity.

https://doi.org/10.1021/jacs.2c08258
J. Am. Chem. Soc. XXXX, XXX, XXX−XXX

CONCLUSIONS

In summary, for the first time, we reported the design and synthesis of a series of stable thorium clusters (**Th_6-MA**, **Th_6-BEN**, **Th_6-C8A**, and **Th_6-Fcc**) coordinated by switchable functional ligands and investigated their role as catalysts in photo/thermodriven amine oxidation reactions in detail. In the photocatalytic oxidative coupling of benzylamine, **Th_6-C8A** was expected to be the best heterogeneous catalyst among four thorium clusters owing to its strong charge separation ability and adsorption capacity to the substrate, which can reach >99% selectivity and approximately 100% conversion in visible light. In aniline oxidation, the selectivity of aniline oxidation products can be regulated by thorium clusters functionalized with different capping ligands, and significant selectivity and conversion of products are achieved. Noteworthy, this is the first time that the selective regulation of four products (including AOB, AB, NSB, and NB) has been achieved using a model crystalline cluster-based catalyst system. Afterward, DFT calculations also revealed the role of thorium clusters in amine oxidation, which may activate O_2/H_2O_2 and thus generate specific reactive species for efficient conversion of amines. This work provides an important case study for the development and application of thorium clusters in the fields of photocatalysis and thermocatalysis.

ASSOCIATED CONTENT

Supporting Information

The Supporting Information is available free of charge at https://pubs.acs.org/doi/10.1021/jacs.2c08258.

Detailed information regarding the experimental methods, characterization analysis, DFT calculations, and CIF file (PDF)

Accession Codes

CCDC 2180693, 2180696, and 2180782 contain the supplementary crystallographic data for this paper. These data can be obtained free of charge via www.ccdc.cam.ac.uk/data_request/cif, or by emailing data_request@ccdc.cam.ac.uk, or by contacting The Cambridge Crystallographic Data Centre, 12 Union Road, Cambridge CB2 1EZ, UK; fax: +44 1223 336033.

AUTHOR INFORMATION

Corresponding Authors

Jiang Liu − *School of Chemistry, South China Normal University, Guangzhou 510006, P. R. China;* orcid.org/0000-0002-2596-4928; Email: liuj0828@m.scnu.edu.cn, liuj@njnu.edu.cn

Ya-Qian Lan − *Jiangsu Collaborative Innovation Centre of Biomedical Functional Materials, Jiangsu Key Laboratory of New Power Batteries, School of Chemistry and Materials Science, Nanjing Normal University, Nanjing 210023, P. R. China; School of Chemistry, South China Normal University, Guangzhou 510006, P. R. China;* orcid.org/0000-0002-2140-7980; Email: yqlan@m.scnu.edu.cn, yqlan@njnu.edu.cn

Authors

Qian Niu − *Jiangsu Collaborative Innovation Centre of Biomedical Functional Materials, Jiangsu Key Laboratory of New Power Batteries, School of Chemistry and Materials Science, Nanjing Normal University, Nanjing 210023, P. R. China*

Qing Huang − *School of Chemistry, South China Normal University, Guangzhou 510006, P. R. China*

Tao-Yuan Yu − *Jiangsu Collaborative Innovation Centre of Biomedical Functional Materials, Jiangsu Key Laboratory of New Power Batteries, School of Chemistry and Materials Science, Nanjing Normal University, Nanjing 210023, P. R. China*

Jing-Wen Shi − *Jiangsu Collaborative Innovation Centre of Biomedical Functional Materials, Jiangsu Key Laboratory of New Power Batteries, School of Chemistry and Materials Science, Nanjing Normal University, Nanjing 210023, P. R. China*

Long-Zhang Dong − *School of Chemistry, South China Normal University, Guangzhou 510006, P. R. China;* orcid.org/0000-0002-9276-5101

Shun-Li Li − *School of Chemistry, South China Normal University, Guangzhou 510006, P. R. China*

Complete contact information is available at: https://pubs.acs.org/10.1021/jacs.2c08258

Author Contributions

Q.N., Q.H., and T.-Y.Y. contributed equally to this work. All authors have approved the final version of the manuscript.

Notes

The authors declare no competing financial interest.

ACKNOWLEDGMENTS

This study was financially supported by the National Science Foundation for Distinguished Young Scholars (22225109), the National Natural Science Foundation of China (Nos. 92061101 and 22271104), Excellent Youth Foundation of Jiangsu Natural Science Foundation (No. BK20211593), and Foundation of Jiangsu Collaborative Innovation Center of Biomedical Functional Materials.

REFERENCES

(1) Lu, H.; Xu, M.; Zheng, Z.; Liu, Q.; Qian, J.; Zhang, Z. H.; He, M. Y.; Qian, Y.; Wang, J. Q.; Lin, J. Emergence of Thorium-Based Polyoxo Clusters as a Platform for Selective X-ray Dosimetry. *Inorg. Chem.* **2021**, *60*, 18629−18633.

(2) Humphrey, U. E.; Khandaker, M. U. Viability of thorium-based nuclear fuel cycle for the next generation nuclear reactor: Issues and prospects. *Renewable Sustainable Energy Rev.* **2018**, *97*, 259−275.

(3) Wang, Z.; Brown, A. T.; Tan, K.; Chabal, Y. J.; Balkus, K. J., Jr. Selective Extraction of Thorium from Rare Earth Elements Using Wrinkled Mesoporous Carbon. *J. Am. Chem. Soc.* **2018**, *140*, 14735−14739.

(4) Cheisson, T.; Kersey, K. D.; Mahieu, N.; McSkimming, A.; Gau, M. R.; Carroll, P. J.; Schelter, E. J. Multiple Bonding in Lanthanides and Actinides: Direct Comparison of Covalency in Thorium(IV)- and Cerium(IV)-Imido Complexes. *J. Am. Chem. Soc.* **2019**, *141*, 9185−9190.

(5) Settineri, N. S.; Garner, M. E.; Arnold, J. A Thorium Chalcogenolate Series Generated by Atom Insertion into Thorium-Carbon Bonds. *J. Am. Chem. Soc.* **2017**, *139*, 6261−6269.

(6) Arnold, P. L.; Ochiai, T.; Lam, F. Y. T.; Kelly, R. P.; Seymour, M. L.; Maron, L. Metallacyclic actinide catalysts for dinitrogen conversion to ammonia and secondary amines. *Nat. Chem.* **2020**, *12*, 654−659.

(7) Bell, N. L.; Maron, L.; Arnold, P. L. Thorium Mono- and Bis(imido) Complexes Made by Reprotonation of cyclo-Metalated Amides. *J. Am. Chem. Soc.* **2015**, *137*, 10492−10495.

(8) Hsueh, F. C.; Barluzzi, L.; Keener, M.; Rajeshkumar, T.; Maron, L.; Scopelliti, R.; Mazzanti, M. Reactivity of Multimetallic Thorium

Nitrides Generated by Reduction of Thorium Azides. *J. Am. Chem. Soc.* **2022**, *144*, 3222−3232.
(9) Rheinfrank, E.; Portner, M.; Nunez Beyerle, M. D. C.; Haag, F.; Deimel, P. S.; Allegretti, F.; Seufert, K.; Barth, J. V.; Bocquet, M. L.; Feulner, P.; Auwarter, W. Actinide Coordination Chemistry on Surfaces: Synthesis, Manipulation, and Properties of Thorium Bis(porphyrinato) Complexes. *J. Am. Chem. Soc.* **2021**, *143*, 14581−14591.
(10) Li, Z. J.; Guo, X.; Qiu, J.; Lu, H.; Wang, J. Q.; Lin, J. Recent advances in the applications of thorium-based metal-organic frameworks and molecular clusters. *Dalton Trans.* **2022**, *51*, 7376−7389.
(11) Ok, K. M.; Sung, J.; Hu, G.; Jacobs, R. M. J.; O'Hare, D. TOF-2: A Large 1D Channel Thorium Organic Framework. *J. Am. Chem. Soc.* **2008**, *130*, 3762−3763.
(12) Andreo, J.; Priola, E.; Alberto, G.; Benzi, P.; Marabello, D.; Proserpio, D. M.; Lamberti, C.; Diana, E. Autoluminescent Metal-Organic Frameworks (MOFs): Self-Photoemission of a Highly Stable Thorium MOF. *J. Am. Chem. Soc.* **2018**, *140*, 14144−14149.
(13) Gilson, S. E.; Fairley, M.; Julien, P.; Oliver, A. G.; Hanna, S. L.; Arntz, G.; Farha, O. K.; LaVerne, J. A.; Burns, P. C. Unprecedented Radiation Resistant Thorium-Binaphthol Metal-Organic Framework. *J. Am. Chem. Soc.* **2020**, *142*, 13299−13304.
(14) Ju, Y.; Li, Z. J.; Lu, H.; Zhou, Z.; Li, Y.; Wu, X. L.; Guo, X.; Qian, Y.; Zhang, Z. H.; Lin, J.; Wang, J. Q.; He, M. Y. Interpenetration Control in Thorium Metal-Organic Frameworks: Structural Complexity toward Iodine Adsorption. *Inorg. Chem.* **2021**, *60*, 5617−5626.
(15) Li, Y.; Yang, Z.; Wang, Y.; Bai, Z.; Zheng, T.; Dai, X.; Liu, S.; Gui, D.; Liu, W.; Chen, M.; Chen, L.; Diwu, J.; Zhu, L.; Zhou, R.; Chai, Z.; Albrecht-Schmitt, T. E.; Wang, S. A mesoporous cationic thorium-organic framework that rapidly traps anionic persistent organic pollutants. *Nat. Commun.* **2017**, *8*, 1354.
(16) Li, Z. J.; Yue, Z.; Ju, Y.; Wu, X.; Ren, Y.; Wang, S.; Li, Y.; Zhang, Z. H.; Guo, X.; Lin, J.; Wang, J. Q. Ultrastable Thorium Metal-Organic Frameworks for Efficient Iodine Adsorption. *Inorg. Chem.* **2020**, *59*, 4435−4442.
(17) Wang, Y.; Liu, W.; Bai, Z.; Zheng, T.; Silver, M. A.; Li, Y.; Wang, Y.; Wang, X.; Diwu, J.; Chai, Z.; Wang, S. Employing an Unsaturated Th$^{(4+)}$ Site in a Porous Thorium-Organic Framework for Kr/Xe Uptake and Separation. *Angew. Chem., Int. Ed.* **2018**, *57*, 5783−5787.
(18) Dolgopolova, E. A.; Ejegbavwo, O. A.; Martin, C. R.; Smith, M. D.; Setyawan, W.; Karakalos, S. G.; Henager, C. H.; Zur Loye, H. C.; Shustova, N. B. Multifaceted Modularity: A Key for Stepwise Building of Hierarchical Complexity in Actinide Metal-Organic Frameworks. *J. Am. Chem. Soc.* **2017**, *139*, 16852−16861.
(19) Ejegbavwo, O. A.; Martin, C. R.; Olorunfemi, O. A.; Leith, G. A.; Ly, R. T.; Rice, A. M.; Dolgopolova, E. A.; Smith, M. D.; Karakalos, S. G.; Birkner, N.; Powell, B. A.; Pandey, S.; Koch, R. J.; Misture, S. T.; Loye, H. Z.; Phillpot, S. R.; Brinkman, K. S.; Shustova, N. B. Thermodynamics and Electronic Properties of Heterometallic Multinuclear Actinide-Containing Metal-Organic Frameworks with "Structural Memory". *J. Am. Chem. Soc.* **2019**, *141*, 11628−11640.
(20) Liu, H.; Khononov, M.; Eisen, M. S. Catalytic 1,2-Regioselective Dearomatization of *N*-Heteroaromatics via a Hydroboration. *ACS Catal.* **2018**, *8*, 3673−3677.
(21) Lv, K.; Fichter, S.; Gu, M.; März, J.; Schmidt, M. An updated status and trends in actinide metal-organic frameworks (An-MOFs): From synthesis to application. *Coord. Chem. Rev.* **2021**, *446*, No. 214011.
(22) Makarov, K.; Kaushansky, A.; Eisen, M. S. Catalytic Hydroboration of Esters by Versatile Thorium and Uranium Amide Complexes. *ACS Catal.* **2022**, *12*, 273−284.
(23) Saha, S.; Eisen, M. S. Catalytic Recycling of a Th−H Bond via Single or Double Hydroboration of Inactivated Imines or Nitriles. *ACS Catal.* **2019**, *9*, 5947−5956.
(24) Huang, Z. W.; Hu, K. Q.; Mei, L.; Kong, X. H.; Yu, J. P.; Liu, K.; Zeng, L. W.; Chai, Z. F.; Shi, W. Q. A mixed-ligand strategy regulates thorium-based MOFs. *Dalton Trans.* **2020**, *49*, 983−987.
(25) Li, P.; Goswami, S.; Otake, K. I.; Wang, X.; Chen, Z.; Hanna, S. L.; Farha, O. K. Stabilization of an Unprecedented Hexanuclear Secondary Building Unit in a Thorium-Based Metal-Organic Framework. *Inorg. Chem.* **2019**, *58*, 3586−3590.
(26) Xu, H.; Cao, C. S.; Hu, H. S.; Wang, S. B.; Liu, J. C.; Cheng, P.; Kaltsoyannis, N.; Li, J.; Zhao, B. High Uptake of ReO_4^- and CO_2 Conversion by a Radiation-Resistant Thorium-Nickle $[Th_{48}Ni_6]$ Nanocage-Based Metal-Organic Framework. *Angew. Chem., Int. Ed.* **2019**, *58*, 6022−6027.
(27) Lu, H.; Xie, J.; Wang, X. Y.; Wang, Y.; Li, Z. J.; Diefenbach, K.; Pan, Q. J.; Qian, Y.; Wang, J. Q.; Wang, S.; Lin, J. Visible colorimetric dosimetry of UV and ionizing radiations by a dual-module photochromic nanocluster. *Nat. Commun.* **2021**, *12*, 2798.
(28) Torapava, N.; Persson, I.; Eriksson, L.; Lundberg, D. Hydration and hydrolysis of thorium(IV) in aqueous solution and the structures of two crystalline thorium(IV) hydrates. *Inorg. Chem.* **2009**, *48*, 11712−11723.
(29) Jantunen, K. C.; Scott, B. L.; Kiplinger, J. L. A comparative study of the reactivity of Zr(IV), Hf(IV) and Th(IV) metallocene complexes: Thorium is not a Group IV metal after all. *J. Alloys Compd.* **2007**, *444-445*, 363−368.
(30) Qian, X. Y.; Zhou, T. H.; Mao, J. G. New thorium(iv)-arsonates with a $[Th_8O_{13}]^{6+}$ octanuclear core. *Dalton Trans.* **2015**, *44*, 13573−13580.
(31) Travia, N. E.; Scott, B. L.; Kiplinger, J. L. A rare tetranuclear thorium(IV) mu_4-oxo cluster and dinuclear thorium(IV) complex assembled by carbon-oxygen bond activation of 1,2-dimethoxyethane (DME). *Chem. − Eur. J.* **2014**, *20*, 16846−16852.
(32) Tsantis, S. T.; Lagou-Rekka, A.; Konidaris, K. F.; Raptopoulou, C. P.; Bekiari, V.; Psycharis, V.; Perlepes, S. P. Tetranuclear oxido-bridged thorium(iv) clusters obtained using tridentate Schiff bases. *Dalton Trans.* **2019**, *48*, 15668−15678.
(33) Li, P.; Wang, X.; Otake, K.-i.; Lyu, J.; Hanna, S. L.; Islamoglu, T.; Farha, O. K. Synthetic Control of Thorium Polyoxo-Clusters in Metal−Organic Frameworks toward New Thorium-Based Materials. *ACS Appl. Nano Mater.* **2019**, *2*, 2260−2265.
(34) Lu, H.; Hou, H.; Hou, Y. C.; Zheng, Z.; Ma, Y.; Zhou, Z.; Guo, X.; Pan, Q. J.; Wang, Y.; Qian, Y.; Wang, J. Q.; Lin, J. A New Concept of Radiation Detection Based on a Fluorochromic and Piezochromic Nanocluster. *J. Am. Chem. Soc.* **2022**, *144*, 3449−3457.
(35) Knope, K. E.; Vasiliu, M.; Dixon, D. A.; Soderholm, L. Thorium(IV)-selenate clusters containing an octanuclear Th(IV) hydroxide/oxide core. *Inorg. Chem.* **2012**, *51*, 4239−4249.
(36) Zhang, M.; Yu, Z.; Xiong, J.; Zhang, R.; Liu, X.; Lu, X. One-step hydrothermal synthesis of $CdxInyS_{(x+1.5y)}$ for photocatalytic oxidation of biomass-derived 5-hydroxymethylfurfural to 2, 5-diformylfuran under ambient conditions. *Appl. Catal., B* **2022**, *300*, No. 120738.
(37) Johnson, J. A.; Luo, J.; Zhang, X.; Chen, Y.-S.; Morton, M. D.; Echeverría, E.; Torres, F. E.; Zhang, J. Porphyrin-Metalation-Mediated Tuning of Photoredox Catalytic Properties in Metal−Organic Frameworks. *ACS Catal.* **2015**, *5*, 5283−5291.
(38) Liu, H.; Xu, C.; Li, D.; Jiang, H. L. Photocatalytic Hydrogen Production Coupled with Selective Benzylamine Oxidation over MOF Composites. *Angew. Chem., Int. Ed.* **2018**, *57*, 5379−5383.
(39) Lv, M.; Tong, F.; Wang, Z.; Liu, Y.; Wang, P.; Cheng, H.; Dai, Y.; Zheng, Z.; Huang, B. $BiVO_4$ quadrangular nanoprisms with highly exposed {101} facets for selective photocatalytic oxidation of benzylamine. *J. Mater. Chem. A* **2022**, DOI: 10.1039/d2ta01758j.
(40) Xiao, Y.; Tian, G.; Li, W.; Xie, Y.; Jiang, B.; Tian, C.; Zhao, D.; Fu, H. Molecule Self-Assembly Synthesis of Porous Few-Layer Carbon Nitride for Highly Efficient Photoredox Catalysis. *J. Am. Chem. Soc.* **2019**, *141*, 2508−2515.
(41) Chen, H.; Liu, C.; Guo, W.; Wang, Z.; Shi, Y.; Yu, Y.; Wu, L. Functionalized UiO-66(Ce) for photocatalytic organic transformation: the role of active sites modulated by ligand functionalization. *Catal. Sci. Technol.* **2022**, *12*, 1812−1823.
(42) Li, S.; Li, L.; Li, Y.; Dai, L.; Liu, C.; Liu, Y.; Li, J.; Lv, J.; Li, P.; Wang, B. Fully Conjugated Donor−Acceptor Covalent Organic

https://doi.org/10.1021/jacs.2c08258
J. Am. Chem. Soc. XXXX, XXX, XXX−XXX

Frameworks for Photocatalytic Oxidative Amine Coupling and Thioamide Cyclization. *ACS Catal.* **2020**, *10*, 8717−8726.
(43) Xu, C.; Liu, H.; Li, D.; Su, J. H.; Jiang, H. L. Direct evidence of charge separation in a metal-organic framework: efficient and selective photocatalytic oxidative coupling of amines via charge and energy transfer. *Chem. Sci.* **2018**, *9*, 3152−3158.
(44) Zhao, F. J.; Zhang, G.; Ju, Z.; Tan, Y. X.; Yuan, D. The Combination of Charge and Energy Transfer Processes in MOFs for Efficient Photocatalytic Oxidative Coupling of Amines. *Inorg. Chem.* **2020**, *59*, 3297−3303.
(45) Dutta, B.; Biswas, S.; Sharma, V.; Savage, N. O.; Alpay, S. P.; Suib, S. L. Mesoporous Manganese Oxide Catalyzed Aerobic Oxidative Coupling of Anilines To Aromatic Azo Compounds. *Angew. Chem., Int. Ed.* **2016**, *128*, 2211−2215.
(46) Han, S.; Cheng, Y.; Liu, S.; Tao, C.; Wang, A.; Wei, W.; Yu, H.; Wei, Y. Selective Oxidation of Anilines to Azobenzenes and Azoxybenzenes by a Molecular Mo Oxide Catalyst. *Angew. Chem., Int. Ed.* **2021**, *60*, 6382−6385.
(47) Oseghale, C. O.; Fapojuwo, D. P.; Alimi, O. A.; Akinnawo, C. A.; Mogudi, B. M.; Onisuru, O. R.; Meijboom, R. Bifunctional Cs−Au/Co_3O_4 (Basic and Redox)-Catalyzed Oxidative Synthesis of Aromatic Azo Compounds from Anilines. *Eur. J. Org. Chem.* **2021**, *2021*, 5063−5073.
(48) Qin, J.; Long, Y.; Sun, F.; Zhou, P. P.; Wang, W. D.; Luo, N.; Ma, J. $Zr(OH)_4$-Catalyzed Controllable Selective Oxidation of Anilines to Azoxybenzenes, Azobenzenes and Nitrosobenzenes. *Angew. Chem., Int. Ed.* **2022**, *61*, No. e202112907.
(49) Gontier, S.; Tuel, A. Liquid Phase Oxidation of Anline over Various Transition-Metal-Substituted Molecular Sieves. *J. Catal.* **1995**, *157*, 124−132.
(50) Singh, S. K.; Piscitelli, C. L.; Yamashita, A.; Gouaux, E. Gold-Catalyzed Synthesis of Aromatic Azo Compounds from Anilines and Nitroaromatics. *Science* **2008**, *322*, 1655−1661.
(51) Ghosh, S.; Acharyya, S. S.; Sasaki, T.; Bal, R. Room temperature selective oxidation of aniline to azoxybenzene over a silver supported tungsten oxide nanostructured catalyst. *Green Chem.* **2015**, *17*, 1867−1876.

https://doi.org/10.1021/jacs.2c08258
J. Am. Chem. Soc. XXXX, XXX, XXX−XXX